ACS APPLIED MATERIALS & INTERFACES

Research Article

www.acsami.org

Au@Polymer Core–Shell Nanoparticles for Simultaneously Enhancing Efficiency and Ambient Stability of Organic Optoelectronic Devices

Taesu Kim,[†,‡,§] Hyunbum Kang,[†,‡,§] Seonju Jeong,[‡,⊥] Dong Jin Kang,[†,‡] Changyeon Lee,[†,‡] Chun-Ho Lee,[‡,#] Min-Kyo Seo,[‡,#] Jung-Yong Lee,*[,‡,⊥] and Bumjoon J. Kim*[,†,‡]

[†]Department of Chemical and Biomolecular Engineering, [‡]KI for the NanoCentury, [⊥]Graduate School of Energy, Environment, Water, and Sustainability (EEWS), and [#]Department of Physics, Korea Advanced Institute of Science and Technology (KAIST), Daejeon 305-701, Korea

Supporting Information

ABSTRACT: In this paper, we report and discuss our successful synthesis of monodispersed, polystyrene-coated gold core–shell nanoparticles (Au@PS NPs) for use in highly efficient, air-stable, organic light-emitting diodes (OLEDs) and organic photovoltaics (OPVs). These core–shell NPs retain the dual functions of (1) the plasmonic effect of the Au core and (2) the stability and solvent resistance of the cross-linked PS shell. The monodispersed Au@PS NPs were incorporated into a poly(3,4-ethylenedioxythiophene):poly(styrenesulfonate) (PEDOT:PSS) film that was located between the ITO substrate and the emitting layer (or active layer) in the devices. The incorporation of the Au@PS NPs provided remarkable improvements in the performances of both OLEDs and OPVs, which benefitted from the plasmonic effect of the Au@PS NPs. The OLED device with the Au@PS NPs achieved an enhancement of the current efficiency that was 42% greater than that of the control device. In addition, the power conversion efficiency was increased from 7.6% to 8.4% in PTB7:$PC_{71}BM$-based OPVs when the Au@PS NPs were embedded. Direct evidence of the plasmonic effect on optical enhancement of the device was provided by near-field scanning optical microscopy measurements. More importantly, the Au@PS NPs induced a remarkable and simultaneous improvement in the stabilities of the OLED and OPV devices by reducing the acidic and hygroscopic properties of the PEDOT:PSS layer.

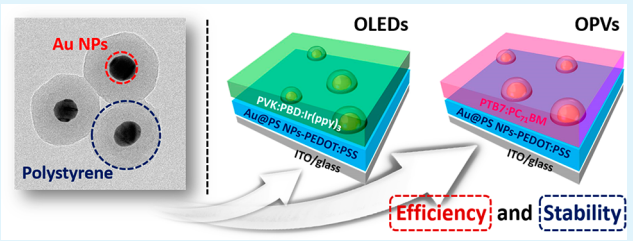

KEYWORDS: *core–shell metal NPs, localized surface plasmon resonance, organic light emitting diodes, organic solar cells, air stability*

INTRODUCTION

Organic optoelectronic devices have attracted a lot of attention in recent years because of their distinct advantages, such as flexibility, low cost, ease of fabrication, and light weight.[1−4] However, the commercialization of the optoelectronic devices, including organic light-emitting diodes (OLEDs) and organic photovoltaics (OPVs), is still limited because of the necessity for further improvement in their efficiencies and long-term stabilities. Much effort has been devoted to improving the efficiency of OLEDs and OPVs, such as the development of new emitting (or active) materials[5−15] and the optimization of film morphologies[16−20] and device structure.[21−28]

Among these attempts, one simple and powerful approach that is applicable for both OLEDs and OPVs is to utilize the localized surface plasmon resonance (LSPR) of metal nanoparticles (NPs). The LSPR effect arises from a localized electromagnetic surface wave at the interface of the metal and dielectric, facilitating light emission and thus enhancing the performance of the OLEDs by accelerating the radiative decay process.[29,30] In addition, the LSPR effect could enhance the light absorption of OPVs from irradiated light via field enhancement near the metal surfaces.[31,32] Particularly, the utilization of Au NPs and Ag NPs is regarded as a promising means that could secure high-efficiency OLEDs and OPVs without modifying the device structure and without increasing the thickness of the emitting or the active layers.[33−43]

To achieve the optimized LSPR effect of metal NPs on the performance of OLED and OPV devices, there are critical requirements for design of the metal NPs. First, controlling the distance between the metal NPs and the emitting layer (or active layer) is very important.[44] The excitons of the emitting layer (or active layer) and the metal NPs must be close to each other to maximize the plasmonic coupling efficiency.[41,45,46] However, the incorporation of the existing organic ligand-capped metal NPs into the organic emitting and active layers in OLEDs and OPVs causes exciton quenching by a nonradiative energy transfer process at the surfaces of the metal NPs.[47] In addition, the surfaces of the metal NPs should be fully protected by stable materials in order to ensure their structural stability against oxidation and to avoid direct contact with the

Received: July 10, 2014
Accepted: September 1, 2014
Published: September 1, 2014

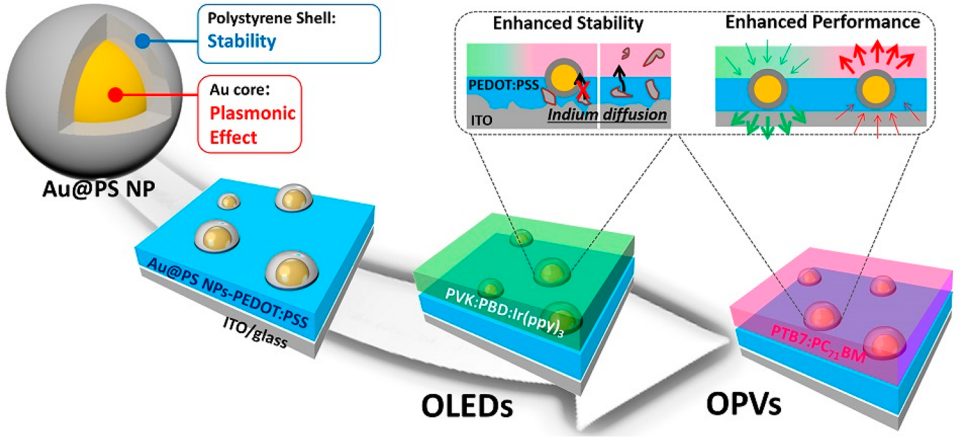

Figure 1. Schematic illustration of our experimental approach using Au@PS NPs for the OLEDs and OPVs. The Au@PS NPs were incorporated in PEDOT:PSS film and then applied for the $Ir(ppy)_3$-based phosphorescent OLEDs and the PTB7-based OPVs as an efficient HIL (or ABL). Both the efficiency and stability of the OLED and OPV devices were simultaneously enhanced by using the Au@PS NPs.

active layer, thus ensuring the stability of the OLED and OPV devices.[48] For these reasons, the optimization of the plasmonic effect for producing highly efficient optoelectronic devices is significantly influenced by the surface properties of the metal NPs. It remains very challenging to develop a proper design for metal NPs with a protective shell that has the desired thickness and superior structural stability.

A metal−polymer, core−shell type NP strategy could be a key solution for addressing these issues. The chemically stable nature of a polymeric shell on the core−shell type NPs could effectively prevent the excitons in the emitting layer of the OLEDs (or the active layer of the OPVs) from being quenched on the surface of the metal core. More importantly, the thickness of the shell can be adjusted easily, allowing precise control of the distance between the metal core and the emitting layer (or active layer) to optimize the plasmonic effect of the metal NPs in OLEDs and OPVs.[49,50] And, the polymeric shell can block the oxidation of the metal NPs by shielding them from oxidants. Furthermore, if the core−shell NPs have a uniform size, they could generate a template for a conducting PEDOT:PSS films with minimal amount of PEDOT:PSS polymers, which can significantly improve the long-term stability of high-performance, organic optoelectronic devices.[51,52] For example, we recently demonstrated the use of monodispersed polystyrene nanoparticles (PS NPs) as a template for producing conducting PEDOT:PSS films and demonstrated their successful application as an anode buffer layer (ABL) in OPVs.[53] The template reduced the amount of PEDOT:PSS significantly in the ABL, and that dramatically improved the long-term stability of the OPVs by alleviating the acidic and hygroscopic environments of the ABL.[54−57] For the above reasons, the development of monodispersed, metal−polymer, core−shell NPs could be a powerful solution for achieving both enhanced efficiency and long-term stability in both OLEDs and OPVs.

Herein, we developed Au core-PS shell nanoparticles (Au@PS NPs) for application in OLEDs and OPVs that achieve high efficiency with enhanced long-term stability. The monodispersed Au@PS NPs with cross-linked PS shells were synthesized and incorporated into PEDOT:PSS films to generate the plasmonic effect of the Au@PS NPs in OLEDs and OPVs (Figure 1). It was observed that the utilization of Au@PS NPs was capable of generating OLEDs and OPVs that exhibited superior performance and long-term stability. The enhanced performances of the OLEDs and OPVs were attributed to the LSPR effect of the Au@PS NPs, and this was supported by the results obtained from near-field scanning optical microscopy (NSOM) and other optical measurements, including photoluminescence (PL), electroluminescence (EL) and spectral absorbance. Finally, we also investigated the effect of Au@PS NPs on improving the ambient stability of OLEDs and OPVs. It was notable and important that the use of Au@PS NPs remarkably enhanced the long-term stabilities of OLEDs and OPVs (in terms of their half-lives) by factors of 1.7 and 3.5, respectively, compared to the control devices.

EXPERIMENTAL SECTION

Materials. $HAuCl_4$, sodium citrate tribasic dihydrate, poly(vinylpyrrolidone) (PVP) (M_w = 55 000 g/mol), divinylbenzene (DVB), 2,2′-azobis(2-methylpropionamidine) dihydrochloride (AIBA), styrene, poly(9-vinylcarbazole) (PVK), 2-(4-biphenylyl)-5-phenyl-1,3,4-oxadiazole (PBD), and tris[2-phenylpyridinato-C^2, N]-iridium(III) (Ir(ppy)3) were purchased from Sigma-Aldrich. Commercial PEDOT:PSS in water (AI4083, Clevios), polythieno[3,4-*b*]thiophene/benzodithiophene (PTB7) (1-materials), and $PC_{71}BM$ (Nano-C) were used without further purification.

Synthesis of Monodisperse Au@PS NPs. Au NPs with a core diameter of 34 nm were synthesized using trisodium citrate (Aldrich, 98%) as surfactant in aqueous phase.[58,59] In detail, 0.7 mL of an aqueous sodium citrate solution (1 wt %) in deionized water (DI water) with a resistivity of 18 MΩ cm was added to 100 mL of a hot, aqueous, gold chloride ($HAuCl_4$) solution (1×10^{-2} wt %) to provide the Au NPs. The Au@PS NPs were prepared using the following procedure. First, DI water (19.5 mL) and ethanol (82.5 mL) as a cosolvent system were added to a mixture of styrene (0.95 mL), DVB (0.05 mL) and PVP (300 mg) in a 250 mL, two-necked flask equipped with a reflux condenser and a Teflon-coated magnetic stirring bar. Styrene monomer was purified with aluminum oxide column. The other organic reagents were used without further purification. The reaction mixture was stirred at 70 °C for 1 h under an argon atmosphere prior to styrene polymerization. Then, 3 mL of an aqueous AIBA solution (1.7 wt %) were added to the flask, and, 8 min later, 15 mL of the as-synthesized Au NPs solution (0.01 wt %) were introduced into the reaction mixture. The reaction was continued with heating at 70 °C for another 18 h under an argon atmosphere. The resultant Au@PS NPs were filtered and repeatedly washed by being centrifuged in DI water to remove the residual reactants and PS NPs without Au NPs.

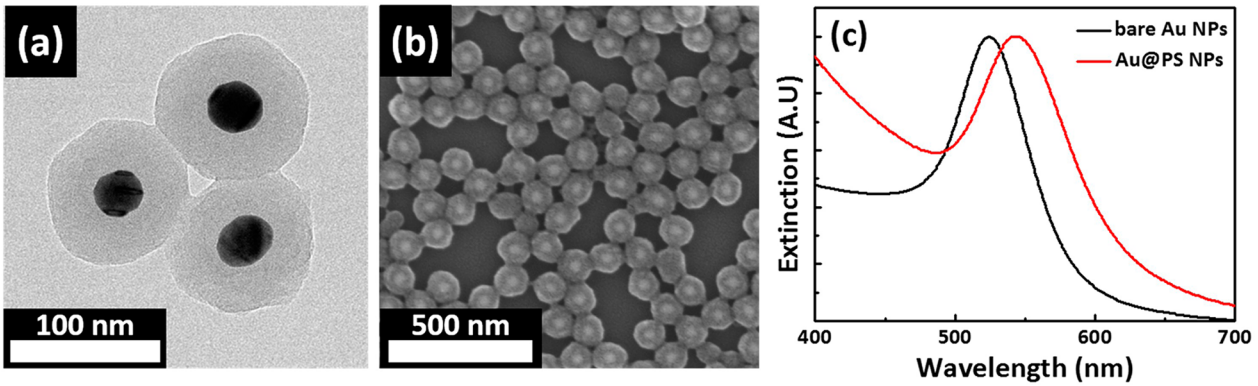

Figure 2. (a) TEM and (b) SEM images of Au@PS NPs; (c) UV−vis absorption spectra of Au NPs (black line) and Au@PS NPs (red line).

Characterization Methods. The extinction spectra of the Au NPs and Au@PS NPs were measured by a UV−vis spectrophotometer (UV-1800, Shimadzu). Field emission scanning electron microscopy (FE-SEM) and transmission electron microscopy (TEM) studies were performed to observe the morphology of Au NPs and Au@PS NPs using a JEOL 2000FX and a Nova230, respectively. The PL spectra were obtained using a Horiba Jobin Yvon NanoLog spectrophotometer with 355 nm as the excitation wavelength. The external quantum efficiency (EQE) curves were obtained by a spectral measurement system (K3100 IQX, McScience Inc.). The light source (a 300-W xenon arc lamp) was used with a monochromator (Newport) and an optical chopper (MC 2000 Thorlabs).

NSOM Measurements. A near-field scanning optical microscope (Alpha300S, WiTec) was used to measure the optical enhancement of the Au@PS NP-incorporated PEDOT:PSS films (Au@PS NP-PEDOT:PSS films) by addition of the Au@PS NPs.[42,60−62] A silicon cantilever with a hollow aluminum pyramid as a tip was used to measure the topography. The detailed NSOM measurement process is as follows. As soon as the NSOM tip approached the sample surface closely, the samples were excited by a Nd:YAG laser (wavelength: 532 nm) that was well-matched with the absorption enhancement region. The NSOM tip captured the evanescent wave while scanning the samples above the PEDOT:PSS surface, and the signals were collected and converted to profile images. The size of the aperture in the tip was 60 nm. The topography and NSOM images were scanned in an area of 2 μm × 2 μm simultaneously. The scanning rate was 1 line/s.

Device Fabrication. Green OLEDs with ITO/Au@PS NP-PEDOT:PSS /PVK:PBD:Ir(ppy)$_3$/LiF/Al and BHJ photovoltaic cells using an ITO/Au@PS NP-PEDOT:PSS/PTB7:PC$_{71}$BM/Ca/Al structure were fabricated. The devices were fabricated on ITO-coated glass substrates with a sheet resistance of 22 Ω/sq. The ITO-coated glass substrates were subjected to ultrasonication in acetone. After the substrates were rinsed extensively with DI water, they were ultrasonicated in DI water, followed by isopropyl alcohol. Subsequently, the substrates were dried completely in an oven at 80 °C. After the substrates were treated with UV-ozone cleaning, PEDOT:PSS films without and with Au@PS NPs were spun onto the substrates at 4000 rpm for 40 s and then annealed at 140 °C for 10 min. In case of OLEDs, a blend solution of PVK:PBD:Ir(ppy)$_3$ ((70:30):2.5 w/w) was dissolved in chlorobenzene and stirred at 80 °C for 1 h. After filtering the blend solution of the emitting materials using a 0.2-μm polytetrafluoroethylene (PTFE) syringe filter, the blend solution was spin-coated to produce a 100 nm-thick film. LiF (1 nm) and Al electrode (100 nm) were evaporated under high vacuum (<1 × 10^{-6} Torr). In case of OPVs, a solution of PTB7 and PC$_{71}$BM was prepared in a chlorobenzene/1,8-diiodooctane (97% to 3%) solution and stirred at 100 °C overnight to ensure complete dissolution of the active materials. The solutions were passed through a 0.45-μm PTFE syringe filter, then spin coated onto the ITO/ABL substrates at 2000 rpm for 35 s. Before evaporation of metal electrode, thermal annealing at 70 °C for 20 min was applied. Ca (20 nm) and Al (100 nm) electrodes were deposited through a shadow mask by thermal evaporation on the devices.

Device Measurement. We measured the performances and the EL spectra of the OLEDs using a current and voltage source meter (Keithley 2400) and a spectroradiometer (Minolta CS-2000). In addition, current density−voltage (J−V) curves of the OPVs were measured by a solar simulator (PEC-L12, Peccell Technologies) under 100 mW/cm^2 from a 150 W Xe short arc lamp filtered by an air mass 1.5 G filter. The intensity of the solar simulator was carefully calibrated using an AIST-certified silicon photodiode.

RESULTS AND DISCUSSION

Synthesis and Characterization of Core−Shell Au@PS NPs. Our Au@PS NPs satisfied important requirements for their use to produce the optimized LSPR effect on the optoelectronic devices with enhanced stability, i.e., (1) the surface plasmon peak of the 34 nm-sized Au@PS NPs in the visible wavelength range can produce high plasmonic interaction with the emitting or active layers for efficient optoelectronic devices; (2) the cross-linked PS shell on the Au@PS NPs must provide excellent structural stability. In addition, the thickness of the PS shell is controllable, making it possible to tune the degree of the plasmonic interaction and thus the plasmonic coupling efficiency between the Au NPs and the emitting or active layers; (3) monodispersed Au@PS NPs that are of comparable in size to the thickness of the PEDOT:PSS film in optimized optoelectronic devices can be self-assembled to generate a template for a conducting PEDOT:PSS film with low percolation thresholds, which can dramatically improve the long-term stability of organic optoelectronic devices.

Considering the above-mentioned critical requirements, we developed a two-step process to produce monodispersed Au@PS NPs. First, Au NPs covered with citrate were prepared using the previously reported procedures.[58,59,63] Then, the Au NPs were encapsulated in PS shells via emulsion polymerization.[49,53] Figure 2 shows the TEM and SEM images of the synthesized Au@PS NPs with a well-defined, core−shell structure. In addition, the Au core was positioned at the center of the Au@PS NPs, showing that the PS shell of the Au@PS NPs was uniformly and completely formed on the Au core. The average diameter of the Au cores was approximately 34 nm, and the total diameter of the Au@PS NPs was approximately 99 nm based on TEM image analysis of more than 400 NPs (see Figure S1 in the Supporting Information). The thickness of the PS shell could provide the suitable distance between the Au core and the emitting layer (or active layer) for the plasmonic organic optoelectronic systems, according to the previous

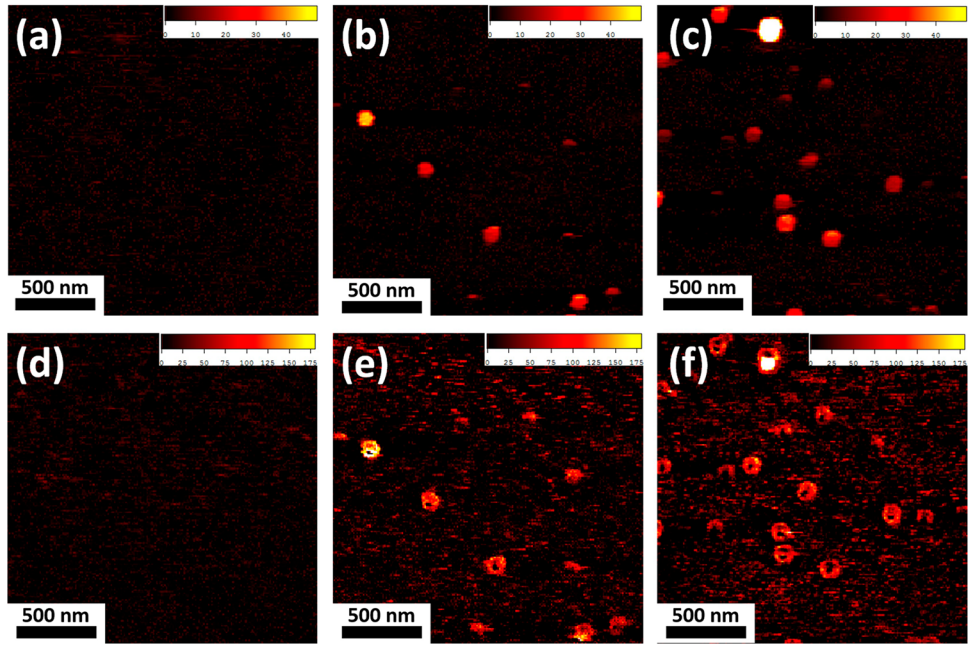

Figure 3. (a–c) NSOM topography images and (d–f) NSOM signal images of PEDOT:PSS films without and with Au@PS NPs. (a, d) Sample 1: N_{NP}= 0/cm^2; (b, e) Sample 3: N_{NP} = 8 × 10^6/cm^2; (c, f) Sample 5: N_{NP} = 1.7 × 10^7/cm^2. NSOM measurement was performed with an excitation of a Nd:YAG laser (532 nm).

report.[44] We noted that the Au@PS NPs coated with PVP surfactants were well dispersed in the PEDOT:PSS film as well as in water without any aggregation. More importantly, the PS shell was cross-linked, providing the Au@PS NPs with resistance to organic solvents. Figure 2c shows the UV–vis absorption spectra of the Au cores and Au@PS NPs dispersed in aqueous solution. When compared to the bare Au cores, the Au@PS NPs exhibited a red-shifted extinction peak at 543 nm, which was caused by the PS shell that had a refractive index of 1.59.[64]

Au@PS NPs for Application in OLEDs and OPVs. To investigate the LSPR effect of Au@PS NPs in the OLEDs and OPVs, we incorporated the synthesized Au@PS NPs into the PEDOT:PSS film, which is located adjacent to the emitting layer in the OLEDs and the active layer of the OPVs. The synthesized Au@PS NPs can be dispersed homogeneously with PEDOT:PSS domains in water, which facilitates the spontaneous fabrication of the Au@PS NP-PEDOT:PSS film using a simple spin-coating process. We controlled the number density (N_{NP}) in the range of 0 to 2.2 × 10^7/cm^2 of Au@PS NPs in the Au@PS NP-PEDOT:PSS films: (Sample 1, 0/cm^2; Sample 2, 3 × 10^6/cm^2; Sample 3, 8 × 10^6/cm^2; Sample 4, 1.3 × 10^7/cm^2; Sample 5, 1.7 × 10^7/cm^2; Sample 6, 2.2 × 10^7/cm^2). The number density of Au@PS NPs in each different sample was obtained by image analysis from more than 50 SEM images. Figure 3a–c compares the NSOM topography images of the pristine PEDOT:PSS (Sample 1), and the Au@PS NP-PEDOT:PSS films (Sample 3, N_{NP} = 8 × 10^6/cm^2 and Sample 5, N_{NP} = 1.7 × 10^7/cm^2). The Au@PS NPs were well-dispersed within a matrix of PEDOT:PSS polymers without any aggregation in Sample 3 and Sample 5.

To provide direct evidence of the optical effect of Au@PS NPs on the optoelectronic devices, we measured a series of Au@PS NP-PEDOT:PSS films with different N_{NP} values in the NSOM collection mode with a Nd:YAG laser (~20 mW) at a wavelength of 532 nm (Figure 3 and Figure S3 in the Supporting Information). Emitting layers (or active layers) were not included in the samples for NSOM measurements. In the NSOM collection mode, the laser was incident from the bottom of the glass substrate to the surface of the PEDOT:PSS film, and near-field signals were collected by the aperture of the NSOM tip. Figure 3d shows that there was no contrast in the intensity in the PEDOT:PSS without Au@PS NPs (Sample 1). On the contrary, images e and f in Figure 3 show that Sample 3 and Sample 5 exhibited a clear contrast between the signal intensities from the PEDOT:PSS regions represented by the black color (low-intensity signal) and the Au@PS NPs regions with the spherical shape, represented by the bright red color (high-intensity signal). Interestingly, the locations of the NSOM signals were in excellent agreement with the locations of the Au@PS NPs in the NSOM topography images. It is suggested that the high-intensity NSOM signals of the Au@PS NPs result from the light scattering caused by the excitation of their surface plasmons. And, the degree of light scattering by Au@PS NPs increased in proportion to the N_{NP} value, and this implied that the performance of the organic optoelectronic devices can depend proportionally on the concentration of the Au@PS NPs.

To demonstrate the applicability of the Au@PS NPs in OLEDs, we fabricated phosphorescent OLEDs using Au@PS NP-PEDOT:PSS films as hole injection layers (HILs). Among the various emitting materials, we chose a green color-emitting material in order to maximize the plasmonic coupling efficiency between the Au@PS NPs and the emitting material and thus fully exploit the use of the Au@PS NPs in the OLEDs.[45] Green OLEDs with the device configuration of glass/ITO/Au@PS NP-PEDOT:PSS/PVK:PBD:Ir(ppy)$_3$/LiF/Al were fabricated with the green-emitting layer consisted of PVK and PBD as hosts and Ir(ppy)$_3$ as a guest.[65] The characteristics of the OLEDs with and without Au@PS NPs are summarized in Table 1. Figure 4a shows the J–V characteristics of the OLEDs without and with Au@PS NPs in the PEDOT:PSS film at the

Table 1. Characteristics of the Green-Emitting and Red-Emitting OLED Devices without (Sample 1: N_{NP} = 0/cm^2) and with Au@PS NPs (Sample 3: N_{NP} = 8 × 10^6/cm^2 and Sample 4: N_{NP} = 1.3 × 10^7/cm^2)

	max. EQE (%) (at voltage)	max. current efficiency (cd/A) (at voltage)	max. power efficiency (lm/W) (at voltage)
		Green-Emissive OLEDs	
sample 1	5.8 (16 V)	20.3 (16 V)	4.5 (13 V)
sample 3	7.3 (15 V)	27.0 (15 V)	5.9 (14 V)
sample 4	7.8 (16 V)	28.9 (16 V)	6.5 (13 V)
		Red-Emissive OLEDs	
sample 1	4.2 (26 V)	3.5 (25 V)	0.5 (22 V)
sample 3	3.8 (25 V)	3.2 (24 V)	0.5 (22 V)
sample 4	3.2 (26 V)	2.7 (26 V)	0.3 (24 V)

optimized N_{NP} value. The current density at a given voltage was slightly improved by embedding the Au@PS NPs in the PEDOT:PSS film. The enhancement in the current density of the devices might be due to the partial reduction of the thickness of the emissive layer from the rough surface caused by the presence of the Au@PS NPs, leading to enhanced electrical field.[66] However, the operating threshold voltages for the OLED devices without and with Au@PS NPs were almost identical (~6 V at 1 cd/m^2). The most distinct differences between the OLEDs without and with Au@PS NPs were the current efficiency and the power efficiency as a function of current density of the OLED devices (Figure 4b). In particular, at the optimum N_{NP} value of 1.3 × 10^7/cm^2, a greatly improved maximum power efficiency of 6.5 lm/W was observed, as opposed to only 4.5 lm/W of the pristine PEDOT:PSS device, which was benefitted from the strong plasmonic coupling effect of the Au@PS NPs with the emitting layer. Similarly, the maximum current efficiency of the device at the N_{NP} value of 1.3 × 10^7/cm^2 increased remarkably by 42%, from 20.3 to 28.9 cd/A, compared to the control device without Au@PS NPs. This showed excellent agreement with the trend in the EQE values of the devices without and with Au@PS NPs, as shown in Table 1. The characteristics of the OLEDs with different values of N_{NP} are summarized in Table S1 in the Supporting Information and shown in Figure S4 in the Supporting Information. When the N_{NP} was increased further to 2.2 × 10^7/cm^2, the maximum current efficiencies and power efficiencies of the OLEDs decreased slightly to 24.6 cd/A and 5.0 lm/W, respectively, but the values were still significantly greater than those of the control devices.

Additional evidence for enhanced performance of OLEDs by the LSPR effect of Au@PS NPs was provided by comparing the intensities of the EL and the PL of the OLED devices (Figure 5).[29,30,39] The EL intensities of the devices were measured at a constant current density of 5 mA/cm^2, and the PL intensities of the samples with the configuration of ITO/Au@PS NP-PEDOT:PSS/PVK:PBD:Ir(ppy)$_3$ were compared when excited by the laser at the wavelength of 355 nm. This excitation wavelength is very far from the resonance frequency (540 nm) of the Au@PS NPs, which avoids the possibility of the simultaneous excitation of the NPs and the emitter. The EL intensity with Au@PS NPs in the wavelength range of 490 to 580 nm showed a remarkable enhancement of 50% over that of the control device (Figure 5a). The results indicated that the improvement in the OLED performance was attributed mainly to the LSPR effect between the emitter and the Au@PS NPs. To further prove that the improvement of the OLED

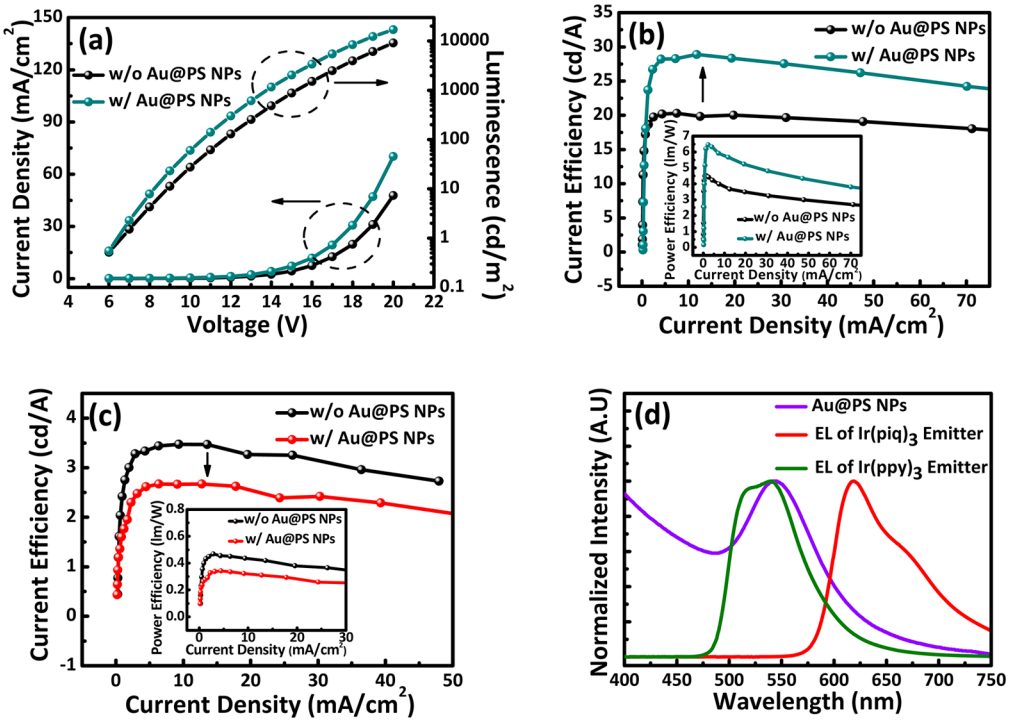

Figure 4. (a) Current density (mA/cm^2) and luminescence (cd/m^2) versus driving voltage; (b) current efficiency (cd/A) and power efficiency (lm/W) (inset) versus current density of the Ir(ppy)$_3$-based, green-emitting OLED devices without and with Au@PS NPs (N_{NP} = 1.3 × 10^7 /cm^2); (c) current efficiency (cd/A) and power efficiency (lm/W) (inset) versus current density of the Ir(piq)$_3$-based, red-emitting OLED devices without and with Au@PS (N_{NP} = 1.3 × 10^7 /cm^2); (d) extinction spectra of Au@PS NPs and EL emission spectra of the Ir(ppy)$_3$-based and Ir(piq)$_3$-based OLED devices.

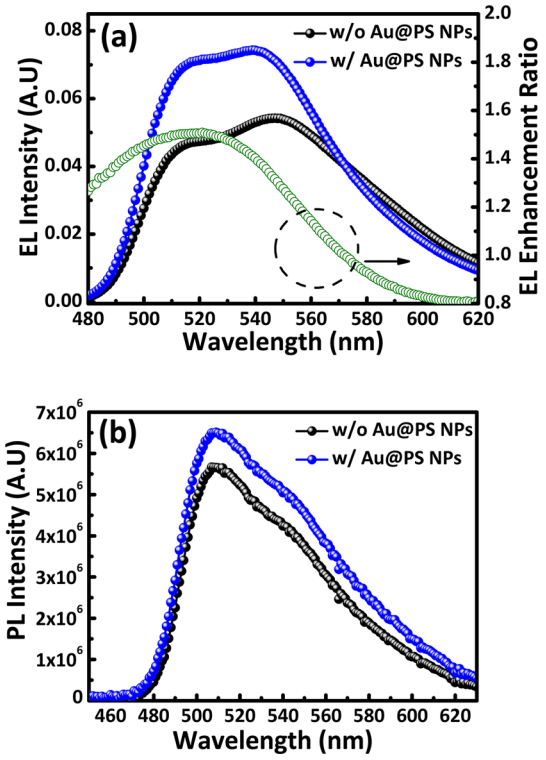

Figure 5. (a) EL spectra of $Ir(ppy)_3$-based OLEDs without and with Au@PS NPs in PEDOT:PSS film at a constant current density of 5 mA/cm^2; (b) PL spectra of $Ir(ppy)_3$-based OLEDs without and with Au@PS NPs in PEDOT:PSS film. Samples for PL measurement were prepared identical to those for EL measurement but without LiF/Al electrode.

performances was attributable mainly to the optical effects of the Au@PS NPs, we also applied the Au@PS NPs to the red color-emitting OLEDs (Figure 4c). The structure of the red-emitting OLED devices was identical to that of the green-emitting OLEDs used in our study, but the red emitters of the $Ir(piq)_3$ were used in the devices.[67] As shown in Table 1 and Figure 4c, the efficiencies of the red-emitting OLED devices were not increased with the addition of the Au@PS NPs; in fact, they were slightly decreased, which was in stark contrast to the trend in the green-emitting devices. Therefore, the enhancement was observed only when the extinction spectrum of the Au@PS NPs was well-matched with the EL spectra of the OLED devices, as shown in Figure 4d.

Au@PS NP-PEDOT:PSS films with different N_{NP} values were compared to elucidate the effect of the Au@PS NPs on the performance of the OPV devices. Several OPV devices were fabricated with an identical ITO/Au@PS NP-PEDOT:PSS film/active layer/Ca/Al structure but different N_{NP} values, ranging from 0/cm^2 to 2.2 × 10^7/cm^2. For the active layer of the OPVs, PTB7, and $PC_{71}BM$ were used for the following reasons: (1) PTB7:$PC_{71}BM$ can absorb light in the range of 400−700 nm, which includes the LSPR region of the Au@PS NPs (450−550 nm) and (2) the PTB7 donor is considered to be the standard system of low band gap polymers for highly efficient OPVs.[9,38] After we prepared a series of Au@PS NP-PEDOT:PSS films with different N_{NP} on ITO glass, the PTB7:$PC_{71}BM$ active layers with the same conditions, including the blend ratio (1:1.5, w/w) and the solution concentration, were spun-cast onto the Au@PS NP-PEDOT:PSS films. The $J-V$ curves and photovoltaic parameters of OPV devices with the full range of N_{NP} values of the Au@PS NPs in PEDOT:PSS film are shown in Figure S5 and Table S2 in the Supporting Information. The PCE values of the OPVs were enhanced and became saturated as the N_{NP} value increased. The best PCE value was remarkably enhanced by 10%, from 7.61% without Au@PS NPs to 8.36% with Au@PS NPs at N_{NP} = 8 × 10^6/cm^2 (Table 2 and Figure 6). This increase was the result of the major improvement of the short-circuit current (J_{sc}) from 15.16 to 16.18 mA/cm^2. And, as shown in the inset in Figure 6b, such enhancement of the J_{SC} value is well reflected in the results of the EQE enhancements. However, the fill factor (FF = 0.67) and the open-circuit voltage (V_{OC} = 0.75) were almost unchanged. When the N_{NP} value exceeded 1.7 × 10^7/cm^2, the PCE value began to decrease. It is noteworthy that, for all N_{NP} values (Samples 2−6), the PCE values of the device with Au@PS NPs were greater than that of the control device without Au@PS NPs. To prove the importance of the optical effect of Au@PS NPs on the OPV performance, we developed a control experiment using the PS NPs (100 nm in diameter, the same as the Au@PS NPs but without the Au core, as shown in Figure S6 in the Supporting Information). A direct comparison between the devices that contained the PS NPs and those that contained the Au@PS NPs at the same N_{NP} values was performed for the case of the PTB7-based OPVs. As shown in Table 2 and Figure 6a, the enhancement in the best OPV performance (PCE = 8.36%) was found only when the Au@PS NPs were incorporated. In contrast, the OPV devices with the PS NPs showed similar PCE value (PCE = 7.38%) compared to the control device (PCE = 7.61%). This trend of similar PCE value by using PS NPs agreed well with our previous report.[53] Thus, it is evident that the Au core in the Au@PS core−shell NPs is a critical component in improving the device performance.

To better understand the LSPR effects of Au@PS NPs on the spectral response in OPVs, we investigated the EQE and absorption spectra of the optimal OPV device with the PS NPs and Au@PS NPs and compared them with the control device (Sample 1), as shown in panels b and c in Figure 6. In the case of the device with Au@PS NPs, EQE and absorbance increased over a broad wavelength range from 390 to 560 nm with almost equal trends. Also, almost identical IQE spectra of the devices

Table 2. Characteristics of PTB7:$PC_{71}BM$ Normal-Type OPVs without Any NPs (Type 1), with PS NPs (Type 2), and with Au@PS NPs (Type 3) in PEDOT:PSS Film under AM 1.5 G-Simulated Solar Illumination (100 mW cm^{-2})[a]

sample (PTB7:$PC_{71}BM$)	V_{OC} (V)	J_{SC} (mA cm^{-2})	FF	PCE (%)[b]
w/o NPs	0.75	15.23 ± 0.09	0.67 ± 0.00	7.59 ± 0.02 (7.61)
w/PS NPs	0.75	14.68 ± 0.10	0.67 ± 0.01	7.35 ± 0.04 (7.38)
w/Au@PS NPs	0.75	16.19 ± 0.03	0.68 ± 0.00	8.27 ± 0.06 (8.36)

[a]N_{NP} values of Au@PS NPs and PS NPs for both Type 2 and Type 3 devices were fixed at 8 × 10^6/cm^2, and both types of NPs were 100 nm in diameter. Average values obtained from at least 8 devices. [b]Value in parentheses illustrates the best cell performance at each device.

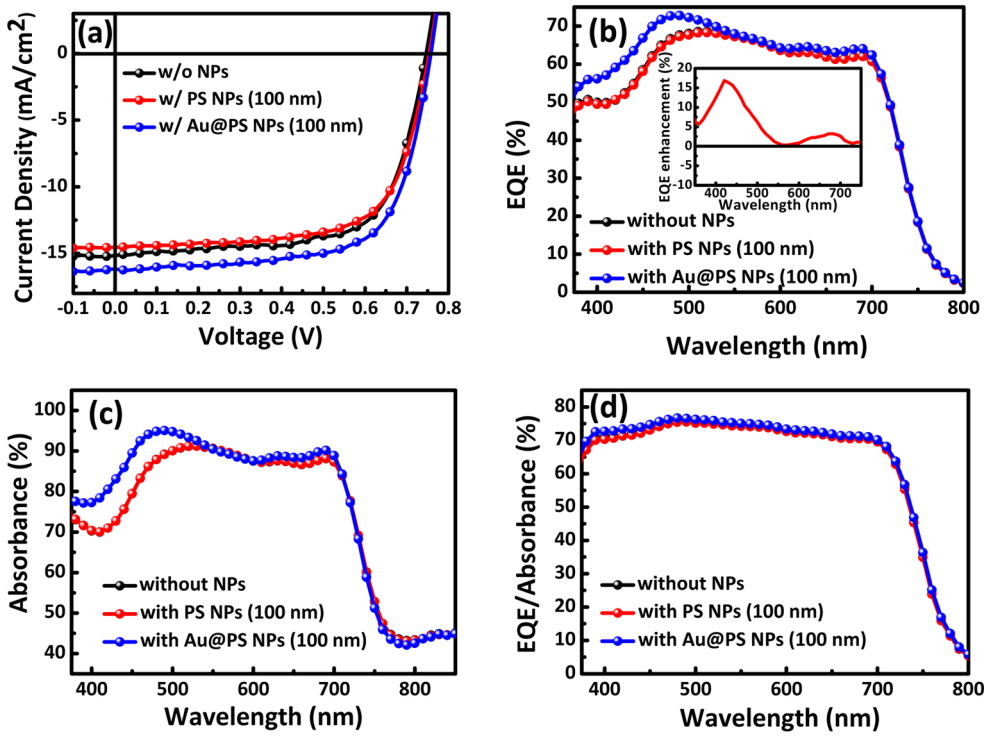

Figure 6. (a) Current density−voltage, (b) external quantum efficiencies (EQEs), (c) absorption, and (d) EQE/absorbance (IQE) characteristics of PTB7:$PC_{71}BM$ normal-type OPVs without and with Au@PS NPs and PS NPs.

without and with Au@PS NPs implied that the EQE enhancement is originated mainly from the enhancement of absorption. However, the maximum extinction spectra of the Au@PS NPs (500−550 nm) did not coincide well with the maximum enhancement range of the EQE spectra (450−500 nm). This was attributed mainly to the feature that the absorption ability and the EQE value of the optimized PTB7:$PC_{71}BM$ device in the range of 500−550 nm were already very high, so the degree of the optical enhancement in the range was rather limited. For this reason, we developed a series of PTB7:$PC_{71}BM$ devices consisting of different D:A (PTB7:$PC_{71}BM$) blend ratios. In general, the modification of the D:A ratio in OPV devices could affect the structures of the EQE curves significantly.[68] For example, as shown in Figure S7a, b in the Supporting Information, when the D:A was changed from the optimum ratio (1:1.5) to the nonoptimum ratio (1:3), the low absorption range was significantly red-shifted from the 400−500 nm range (D:A = 1:1.5) to the 500−600 nm range (D:A = 1:3). In such a case, it was clearly observed that the Au@PS NPs can significantly improve the optical response at a wavelengths of 500−600 nm (see Figure S7c in the Supporting Information), which is very consistent with maximum extinction spectra of the Au@PS NPs.

While achieving long-term stability has been a major hurdle to the commercialization of OLEDs and OPVs, the advantage of the core−shell Au@PS NPs can be highlighted in terms of improving the stabilities of both OLEDs and OPVs. To evaluate the effectiveness of the Au@PS NPs on the stabilities of OLEDs and OPVs, we investigated the air stabilities of the OLEDs and OPVs without and with Au@PS NPs by measuring the efficiencies as a function of the storage time at ambient conditions, as shown in Figure 7. All devices were exposed to air without any encapsulation. First, Figure 7a compares the air stability of the Ir(ppy)$_3$-based, green-emitting OLEDs without

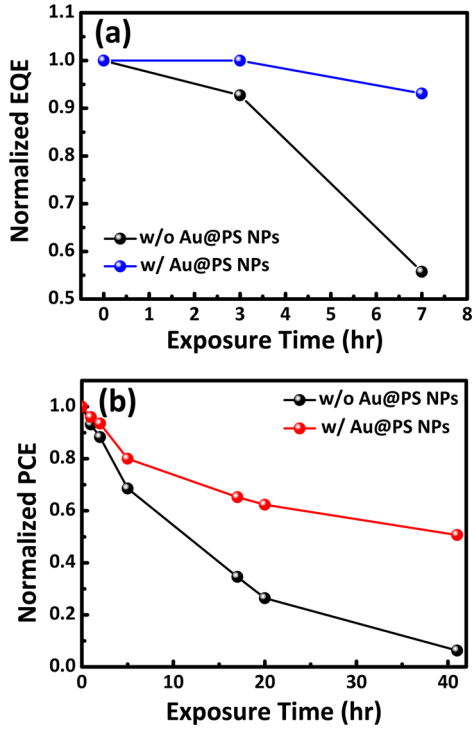

Figure 7. Air stability tests of (a) Ir(ppy)$_3$-based green-emitting OLEDs and (b) PTB7:$PC_{71}BM$ OPVs without and with Au@PS NPs, respectively, measured at ambient conditions.

and with Au@PS NPs. The devices, including the Au@PS NPs, had air stabilities that were remarkably enhanced over those of the control devices. The EQE value of the control device without encapsulation decayed by ∼50% after the device was exposed to air for 420 min. In contrast, the OLEDs with Au@

dx.doi.org/10.1021/am504503q | ACS Appl. Mater. Interfaces 2014, 6, 16956−16965

PS NP-PEDOT:PSS had almost the same performances as the initial EQE value (~94%) after treatment under the same conditions, exhibiting much greater air stability. The effect of Au@PS NPs for the enhancement of air stability was also dramatic for the case of the PTB7:$PC_{71}BM$ OPVs. The PCE value of the control OPV decayed by ~90% after being exposed to air for 2400 min. In contrast, 50% of the initial PCE was retained for the OPV with Au@PS NPs under the same measurement conditions (Figure 7b). The remarkably improved stability was mainly attributed to the Au@PS NPs acting as a barrier, which prevented oxygen diffusion and reduced the degradation of the photoactive and ITO layers by the acidic conditions caused by the PEDOT:PSS polymers. It is well-known that the diffusion of indium from the ITO layer into the emitting layer (or active layer) could be detrimental to the device performance when the PEDOT:PSS film is deposited on ITO.[54,69,70] To confirm this feature, we compared the amount of diffused indium for two different samples, i.e., (1) ITO/pristine PEDOT:PSS (Sample 1) and (2) Au@PS NP-PEDOT:PSS (Sample 6) after seven-day exposures to ambient conditions. The X-ray photoelectron spectroscopy (XPS) measurements in Figure S8 showed that the diffusion of indium in Sample 6 was greatly suppressed compared to that of Sample 1. In addition, it is clearly observed that, as the N_{NP} value increased, the degree of indium diffusion decreased significantly, and, the stability of the devices improved accordingly. Furthermore, we measured and compared the lifetime of the PTB7-based OPVs without any NPs, with the 100 nm-size PS NPs, and the 100 nm-sized Au@PS NPs. Both types of NPs were included in the OPV devices with the same N_{NP} values ($2.2 \times 10^7/cm^2$). We observed that the ambient stabilities of both the devices that contained the PS NPs and those that contained the Au@PS NPs improved significantly with almost same trend, as shown in Figure S9 in the Supporting Information, so the enhancement in the device stability was attributed mainly to the chemically stable PS shell, which can effectively prevent the migration of indium atoms. It was demonstrated that our development of uniform sized Au@PS core−shell NPs is a powerful and versatile approach that can simultaneous enhance both device efficiency and ambient stability for highly efficient OLEDs and OPVs.

CONCLUSIONS

We developed uniform-sized Au@PS NPs to enhance both the efficiency and long-term stability of OLEDs and OPVs. The use of Au@PS NPs induced a simultaneous and remarkable enhancement in the device efficiency and the ambient stability of the OLEDs and OPVs. The enhancement of the device performance was attributed to the LSPR effect of the Au core of the Au@PS NPs. The green emitting OLEDs with the Au@PS NPs achieved a 42% enhancement of their luminous efficiency. In addition, the PCE value of the OPVs with the Au@PS NPs was significantly improved from 7.6% to 8.4%. Direct evidence of the LSPR effect on optical enhancement of the device was provided by the NSOM measurements. More importantly, the air stabilities of both the OLED and OPV devices with the Au@PS NPs were improved significantly. This is the first report of the design and the use of metal−polymer, core−shell NPs in OLEDs and OPVs, resulting in simultaneous improvements of their efficiencies and long-term stabilities.

ASSOCIATED CONTENT

Supporting Information

Characterization data of Au@PS NPs, and detailed device characteristics of OLEDs and OPVs. This material is available free of charge via the Internet at http://pubs.acs.org.

AUTHOR INFORMATION

Corresponding Authors

*E-mail: jungyong.lee@kaist.ac.kr.
*E-mail: bumjoonkim@kaist.ac.kr.

Author Contributions

[§]T.K. and H.K. contributed equally.

Notes

The authors declare no competing financial interest.

ACKNOWLEDGMENTS

This research was supported by the National Research Foundation Grant (2012M1A2A2671746), and by the Global Frontier R&D Program on Center for Multiscale Energy System (2012M3A6A7055540), funded by the Korean Government. This research was supported by the New & Renewable Energy Program of KETEP Grant (20133030000130), funded by the Ministry of Trade, industry & Energy, Republic of Korea. This work is also supported by Graphene Materials and Components Development Program of MOTIE/KEIT (10044412, Development of basic and applied technologies for OLEDs with graphene). The authors also acknowledge Samsung Display Co. and the KAIST EEWS Initiative Research Project (EEWSN01140052) for the financial support.

REFERENCES

(1) Thompson, B. C.; Fréchet, J. M. J. Polymer−Fullerene Composite Solar Cells. *Angew. Chem., Int. Ed.* **2008**, *47*, 58−77.
(2) Shrotriya, V. Organic Photovoltaics: Polymer Power. *Nat. Photonics* **2009**, *3*, 447−449.
(3) Burroughes, J. H.; Bradley, D. D. C.; Brown, A. R.; Marks, R. N.; Mackay, K.; Friend, R. H.; Burns, P. L.; Holmes, A. B. Light Emitting Diodes Based on Conjugated Polymers. *Nature* **1990**, *347*, 539−541.
(4) D'Andrade, B. W.; Forrest, S. R. White Organic Light-Emitting Devices for Solid-State Lighting. *Adv. Mater.* **2004**, *16*, 1585−1595.
(5) Zhang, M.; Guo, X.; Zhang, S.; Hou, J. Synergistic Effect of Fluorination on Molecular Energy Level Modulation in Highly Efficient Photovoltaic Polymers. *Adv. Mater.* **2014**, *26*, 1118−1123.
(6) Cabanetos, C.; El Labban, A.; Bartelt, J. A.; Douglas, J. D.; Mateker, W. R.; Fréchet, J. M. J.; McGehee, M. D.; Beaujuge, P. M. Linear Side Chains in Benzo[1,2-b:4,5-b′]dithiophene−Thieno[3,4-c]pyrrole-4,6-dione Polymers Direct Self-Assembly and Solar Cell Performance. *J. Am. Chem. Soc.* **2013**, *135*, 4656−4659.
(7) Hendriks, K. H.; Heintges, G. H. L.; Gevaerts, V. S.; Wienk, M. M.; Janssen, R. A. J. High-Molecular-Weight Regular Alternating Diketopyrrolopyrrole-based Terpolymers for Efficient Organic Solar Cells. *Angew. Chem., Int. Ed.* **2013**, *52*, 8341−8344.
(8) Kang, T. E.; Cho, H.-H.; Kim, H. j.; Lee, W.; Kang, H.; Kim, B. J. Importance of Optimal Composition in Random Terpolymer-Based Polymer Solar Cells. *Macromolecules* **2013**, *46*, 6806−6813.
(9) Liang, Y.; Xu, Z.; Xia, J.; Tsai, S.-T.; Wu, Y.; Li, G.; Ray, C.; Yu, L. For the Bright Future—Bulk Heterojunction Polymer Solar Cells with Power Conversion Efficiency of 7.4%. *Adv. Mater.* **2010**, *22*, E135−E138.
(10) Sun, Y.; Welch, G. C.; Leong, W. L.; Takacs, C. J.; Bazan, G. C.; Heeger, A. J. Solution-Processed Small-Molecule Solar Cells with 6.7% Efficiency. *Nat. Mater.* **2012**, *11*, 44−48.
(11) Zhong, H.; Li, Z.; Deledalle, F.; Fregoso, E. C.; Shahid, M.; Fei, Z.; Nielsen, C. B.; Yaacobi-Gross, N.; Rossbauer, S.; Anthopoulos, T. D.; Durrant, J. R.; Heeney, M. Fused Dithienogermolodithiophene

Low Band Gap Polymers for High-Performance Organic Solar Cells without Processing Additives. *J. Am. Chem. Soc.* **2013**, *135*, 2040−2043.
(12) He, Y.; Chen, H.-Y.; Hou, J.; Li, Y. Indene−C_{60} Bisadduct: A New Acceptor for High-Performance Polymer Solar Cells. *J. Am. Chem. Soc.* **2010**, *132*, 1377−1382.
(13) Kim, K.-H.; Kang, H.; Nam, S. Y.; Jung, J.; Kim, P. S.; Cho, C.-H.; Lee, C.; Yoon, S. C.; Kim, B. J. Facile Synthesis of o-Xylenyl Fullerene Multiadducts for High Open Circuit Voltage and Efficient Polymer Solar Cells. *Chem. Mater.* **2011**, *23*, 5090−5095.
(14) Zhong, C.; Duan, C.; Huang, F.; Wu, H.; Cao, Y. Materials and Devices toward Fully Solution Processable Organic Light-Emitting Diodes. *Chem. Mater.* **2010**, *23*, 326−340.
(15) Sasabe, H.; Kido, J. Multifunctional Materials in High-Performance OLEDs: Challenges for Solid-State Lighting. *Chem. Mater.* **2010**, *23*, 621−630.
(16) Wang, D. H.; Kyaw, A. K. K.; Pouliot, J.-R.; Leclerc, M.; Heeger, A. J. Enhanced Power Conversion Efficiency of Low Band-Gap Polymer Solar Cells by Insertion of Optimized Binary Processing Additives. *Adv. Energy Mater.* **2014**, *4*, 1300835.
(17) Li, W.; Hendriks, K. H.; Furlan, A.; Roelofs, W. S. C.; Meskers, S. C. J.; Wienk, M. M.; Janssen, R. A. J. Effect of the Fibrillar Microstructure on the Efficiency of High Molecular Weight Diketopyrrolopyrrole-Based Polymer Solar Cells. *Adv. Mater.* **2014**, *26*, 1565−1570.
(18) Ye, L.; Zhang, S.; Ma, W.; Fan, B.; Guo, X.; Huang, Y.; Ade, H.; Hou, J. From Binary to Ternary Solvent: Morphology Fine-tuning of D/A Blends in PDPP3T-based Polymer Solar Cells. *Adv. Mater.* **2012**, *24*, 6335−6341.
(19) Liu, F.; Wang, C.; Baral, J. K.; Zhang, L.; Watkins, J. J.; Briseno, A. L.; Russell, T. P. Relating Chemical Structure to Device Performance via Morphology Control in Diketopyrrolopyrrole-Based Low Band Gap Polymers. *J. Am. Chem. Soc.* **2013**, *135*, 19248−19259.
(20) Li, W.; Hendriks, K. H.; Furlan, A.; Roelofs, W. S. C.; Wienk, M. M.; Janssen, R. A. J. Universal Correlation between Fibril Width and Quantum Efficiency in Diketopyrrolopyrrole-Based Polymer Solar Cells. *J. Am. Chem. Soc.* **2013**, *135*, 18942−18948.
(21) Kim, J. Y.; Lee, K.; Coates, N. E.; Moses, D.; Nguyen, T.-Q.; Dante, M.; Heeger, A. J. Efficient Tandem Polymer Solar Cells Fabricated by All-Solution Processing. *Science* **2007**, *317*, 222−225.
(22) Dou, L.; You, J.; Yang, J.; Chen, C.-C.; He, Y.; Murase, S.; Moriarty, T.; Emery, K.; Li, G.; Yang, Y. Tandem Polymer Solar Cells Featuring a Spectrally Matched Low-Bandgap Polymer. *Nat. Photonics* **2012**, *6*, 180−185.
(23) Li, X. H.; Choy, W. C. H.; Huo, L. J.; Xie, F.; Sha, W. E. I.; Ding, B. F.; Guo, X.; Li, Y. F.; Hou, J. H.; You, J. B.; Yang, Y. Dual Plasmonic Nanostructures for High Performance Inverted Organic Solar Cells. *Adv. Mater.* **2012**, *24*, 3046−3052.
(24) Na, S.-I.; Kim, S.-S.; Jo, J.; Oh, S.-H.; Kim, J.; Kim, D.-Y. Efficient Polymer Solar Cells with Surface Relief Gratings Fabricated by Simple Soft Lithography. *Adv. Funct. Mater.* **2008**, *18*, 3956−3963.
(25) Hyun, W. J.; Lee, H. K.; Oh, S. S.; Hess, O.; Choi, C.-G.; Im, S. H.; Park, O. O. Two-Dimensional TiO_2 Inverse Opal with a Closed Top Surface Structure for Enhanced Light Extraction from Polymer Light-Emitting Diodes. *Adv. Mater.* **2011**, *23*, 1846−1850.
(26) Sun, Y.; Forrest, S. R. Enhanced Light Out-Coupling of Organic Light-Emitting Devices Using Embedded Low-Index Grids. *Nat. Photonics* **2008**, *2*, 483−487.
(27) Kim, J.-B.; Lee, J.-H.; Moon, C.-K.; Kim, S.-Y.; Kim, J.-J. Highly Enhanced Light Extraction from Surface Plasmonic Loss Minimized Organic Light-Emitting Diodes. *Adv. Mater.* **2013**, *25*, 3571−3577.
(28) Kang, D. J.; Kang, H.; Cho, C.; Kim, K.-H.; Jeong, S.; Lee, J.-Y.; Kim, B. J. Efficient Light Trapping in Inverted Polymer Solar Cells by a Randomly Nanostructured Electrode Using Monodispersed Polymer Nanoparticles. *Nanoscale* **2013**, *5*, 1858−1863.
(29) Choi, H.; Ko, S.-J.; Choi, Y.; Joo, P.; Kim, T.; Lee, B. R.; Jung, J.-W.; Choi, H. J.; Cha, M.; Jeong, J.-R.; Hwang, I.-W.; Song, M. H.; Kim, B.-S.; Kim, J. Y. Versatile Surface Plasmon Resonance of Carbon-Dot-Supported Silver Nanoparticles in Polymer Optoelectronic Devices. *Nat. Photonics* **2013**, *7*, 732−738.
(30) Gu, X.; Qiu, T.; Zhang, W.; Chu, P. Light-Emitting Diodes Enhanced by Localized Surface Plasmon Resonance. *Nanoscale Res. Lett.* **2011**, *6*, 199.
(31) Hutter, E.; Fendler, J. H. Exploitation of Localized Surface Plasmon Resonance. *Adv. Mater.* **2004**, *16*, 1685−1706.
(32) Lee, J.-Y.; Peumans, P. The Origin of Enhanced Optical Absorption in Solar Cells with Metal Nanoparticles Embedded in the Active Layer. *Opt. Express* **2010**, *18*, 10078−10087.
(33) Heo, M.; Cho, H.; Jung, J.-W.; Jeong, J.-R.; Park, S.; Kim, J. Y. High-Performance Organic Optoelectronic Devices Enhanced by Surface Plasmon Resonance. *Adv. Mater.* **2011**, *23*, 5689−5693.
(34) Yang, J.; You, J.; Chen, C.-C.; Hsu, W.-C.; Tan, H.-R.; Zhang, X. W.; Hong, Z.; Yang, Y. Plasmonic Polymer Tandem Solar Cell. *ACS Nano* **2011**, *5*, 6210−6217.
(35) Wang, D. H.; Kim, D. Y.; Choi, K. W.; Seo, J. H.; Im, S. H.; Park, J. H.; Park, O. O.; Heeger, A. J. Enhancement of Donor−Acceptor Polymer Bulk Heterojunction Solar Cell Power Conversion Efficiencies by Addition of Au Nanoparticles. *Angew. Chem., Int. Ed.* **2011**, *50*, 5519−5523.
(36) Wang, D. H.; Park, K. H.; Seo, J. H.; Seifter, J.; Jeon, J. H.; Kim, J. K.; Park, J. H.; Park, O. O.; Heeger, A. J. Enhanced Power Conversion Efficiency in PCDTBT/PC_{70}BM Bulk Heterojunction Photovoltaic Devices with Embedded Silver Nanoparticle Clusters. *Adv. Energy Mater.* **2011**, *1*, 766−770.
(37) Wu, J.-L.; Chen, F.-C.; Hsiao, Y.-S.; Chien, F.-C.; Chen, P.; Kuo, C.-H.; Huang, M. H.; Hsu, C.-S. Surface Plasmonic Effects of Metallic Nanoparticles on the Performance of Polymer Bulk Heterojunction Solar Cells. *ACS Nano* **2011**, *5*, 959−967.
(38) Lu, L.; Luo, Z.; Xu, T.; Yu, L. Cooperative Plasmonic Effect of Ag and Au Nanoparticles on Enhancing Performance of Polymer Solar Cells. *Nano Lett.* **2013**, *13*, 59−64.
(39) Xiao, Y.; Yang, J. P.; Cheng, P. P.; Zhu, J. J.; Xu, Z. Q.; Deng, Y. H.; Lee, S. T.; Li, Y. Q.; Tang, J. X. Surface Plasmon-Enhanced Electroluminescence in Organic Light-Emitting Diodes Incorporating Au Nanoparticles. *Appl. Phys. Lett.* **2012**, *100*, 013308.
(40) Ko, S.-J.; Choi, H.; Lee, W.; Kim, T.; Lee, B. R.; Jung, J.-W.; Jeong, J.-R.; Song, M. H.; Lee, J. C.; Woo, H. Y.; Kim, J. Y. Highly Efficient Plasmonic Organic Optoelectronic Devices Based on a Conducting Polymer Electrode Incorporated with Silver Nanoparticles. *Energy Environ. Sci.* **2013**, *6*, 1949−1955.
(41) Janković, V.; Yang, Y.; You, J.; Dou, L.; Liu, Y.; Cheung, P.; Chang, J. P.; Yang, Y. Active Layer-Incorporated, Spectrally Tuned Au/SiO_2 Core/Shell Nanorod-Based Light Trapping for Organic Photovoltaics. *ACS Nano* **2013**, *7*, 3815−3822.
(42) Baek, S.-W.; Noh, J.; Lee, C.-H.; Kim, B.; Seo, M.-K.; Lee, J.-Y. Plasmonic Forward Scattering Effect in Organic Solar Cells: A Powerful Optical Engineering Method. *Sci. Rep.* **2013**, *3*, 1726.
(43) Gu, Y.; Zhang, D.-D.; Ou, Q.-D.; Deng, Y.-H.; Zhu, J.-J.; Cheng, L.; Liu, Z.; Lee, S.-T.; Li, Y.-Q.; Tang, J.-X. Light Extraction Enhancement in Organic Light-Emitting Diodes Based on Localized Surface Plasmon and Light Scattering Double-Effect. *J. Mater. Chem. C* **2013**, *1*, 4319−4326.
(44) Sung, H.; Lee, J.; Han, K.; Lee, J.-K.; Sung, J.; Kim, D.; Choi, M.; Kim, C. Controlled Positioning of Metal Nanoparticles in an Organic Light-Emitting Device for Enhanced Quantum Efficiency. *Org. Electron.* **2014**, *15*, 491−499.
(45) Kumar, A.; Srivastava, R.; Tyagi, P.; Mehta, D. S.; Kamalasanan, M. N. Efficiency Enhancement of Organic Light Emitting Diode via Surface Energy Transfer between Exciton and Surface Plasmon. *Org. Electron.* **2012**, *13*, 159−165.
(46) Liu, F.; Nunzi, J.-M. Phosphorescent Organic Light Emitting Diode Efficiency Enhancement Using Functionalized Silver Nanoparticles. *Appl. Phys. Lett.* **2011**, *99*, 123302.
(47) Wu, B.; Wu, X.; Guan, C.; Fai Tai, K.; Yeow, E. K. L.; Jin Fan, H.; Mathews, N.; Sum, T. C. Uncovering Loss Mechanisms in Silver Nanoparticle-Blended Plasmonic Organic Solar Cells. *Nat. Commun.* **2013**, *4*, 2004.

(48) Choi, H.; Lee, J.-P.; Ko, S.-J.; Jung, J.-W.; Park, H.; Yoo, S.; Park, O.; Jeong, J.-R.; Park, S.; Kim, J. Y. Multipositional Silica-Coated Silver Nanoparticles for High-Performance Polymer Solar Cells. *Nano Lett.* **2013**, *13*, 2204−2208.
(49) Ohnuma, A.; Cho, E. C.; Jiang, M.; Ohtani, B.; Xia, Y. Metal−Polymer Hybrid Colloidal Particles with an Eccentric Structure. *Langmuir* **2009**, *25*, 13880−13887.
(50) Du, X.; He, J. Facile Size-Controllable Syntheses of Highly Monodisperse Polystyrene Nano- and Microspheres by Polyvinylpyrrolidone-Mediated Emulsifier-Free Emulsion Polymerization. *J. Appl. Polym. Sci.* **2008**, *108*, 1755−1760.
(51) Mezzenga, R.; Ruokolainen, J.; Fredrickson, G. H.; Kramer, E. J.; Moses, D.; Heeger, A. J.; Ikkala, O. Templating Organic Semiconductors via Self-Assembly of Polymer Colloids. *Science* **2003**, *299*, 1872−1874.
(52) Kang, D. J.; Kwon, T.; Kim, M. P.; Cho, C.-H.; Jung, H.; Bang, J.; Kim, B. J. Creating Opal-Templated Continuous Conducting Polymer Films with Ultralow Percolation Thresholds Using Thermally Stable Nanoparticles. *ACS Nano* **2011**, *5*, 9017−9027.
(53) Kang, D. J.; Kang, H.; Kim, K.-H.; Kim, B. J. Nanosphere Templated Continuous PEDOT:PSS Films with Low Percolation Threshold for Application in Efficient Polymer Solar Cells. *ACS Nano* **2012**, *6*, 7902−7909.
(54) Reese, M. O.; Morfa, A. J.; White, M. S.; Kopidakis, N.; Shaheen, S. E.; Rumbles, G.; Ginley, D. S. Pathways for the Degradation of Organic Photovoltaic P3HT:PCBM Based Devices. *Sol. Energy Mater. Sol. Cells* **2008**, *92*, 746−752.
(55) Watanabe, A.; Kasuya, A. Effect of Atmospheres on the Open-Circuit Photovoltage of Nanoporous TiO_2/poly(3-hexylthiophene) Heterojunction Solar Cell. *Thin Solid Films* **2005**, *483*, 358−366.
(56) Şahin, Y.; Alem, S.; de Bettignies, R.; Nunzi, J.-M. Development of Air Stable Polymer Solar Cells Using an Inverted Gold on Top Anode Structure. *Thin Solid Films* **2005**, *476*, 340−343.
(57) Fehse, K.; Meerheim, R.; Walzer, K.; Leo, K.; Lovenich, W.; Elschner, A. Lifetime of Organic Light Emitting Diodes on Polymer Anodes. *Appl. Phys. Lett.* **2008**, *93*, 083303.
(58) Turkevich, J.; Stevenson, P. C.; Hillier, J. A Study of the Nucleation and Growth Processes in the Synthesis of Colloidal Gold. *Discuss. Faraday Soc.* **1951**, *11*, 55−75.
(59) Frens, G. Controlled Nucleation for the Regulation of the Particle Size in Monodisperse Gold Suspensions. *Nature* **1973**, *241*, 20−22.
(60) Benrezzak, S.; Adam, P. M.; Bijeon, J. L.; Royer, P. Observation of Nanometric Metallic Particles with an Apertureless Scanning Near-field Optical Microscope. *Surf. Sci.* **2001**, *491*, 195−207.
(61) Prikulis, J.; Xu, H.; Gunnarsson, L.; Käll, M.; Olin, H. Phase-Sensitive Near-Field Imaging of Metal Nanoparticles. *J. Appl. Phys.* **2002**, *92*, 6211−6214.
(62) Chang, Y.-C.; Chen, H.-W.; Chang, S.-H. Enhanced Near-Field Imaging Contrasts of Silver Nanoparticles by Localized Surface Plasmon. *IEEE J. Sel. Top. Quantum Electron.* **2008**, *14*, 1536−1539.
(63) Kimling, J.; Maier, M.; Okenve, B.; Kotaidis, V.; Ballot, H.; Plech, A. Turkevich Method for Gold Nanoparticle Synthesis Revisited. *J. Phys. Chem. B* **2006**, *110*, 15700−15707.
(64) Bardhan, R.; Grady, N. K.; Halas, N. J. Nanoscale Control of Near-Infrared Fluorescence Enhancement Using Au Nanoshells. *Small* **2008**, *4*, 1716−1722.
(65) Earmme, T.; Ahmed, E.; Jenekhe, S. A. Highly Efficient Phosphorescent Light-Emitting Diodes by Using an Electron-Transport Material with High Electron Affinity. *J. Phys. Chem. C* **2009**, *113*, 18448−18450.
(66) Fujita, M.; Ueno, T.; Ishihara, K.; Asano, T.; Noda, S.; Ohata, H.; Tsuji, T.; Nakada, H.; Shimoji, N. Reduction of Operating Voltage in Organic Light-Emitting Diode by Corrugated Photonic Crystal Structure. *Appl. Phys. Lett.* **2004**, *85*, 5769−5771.
(67) Tsuboyama, A.; Iwawaki, H.; Furugori, M.; Mukaide, T.; Kamatani, J.; Igawa, S.; Moriyama, T.; Miura, S.; Takiguchi, T.; Okada, S.; Hoshino, M.; Ueno, K. Homoleptic Cyclometalated Iridium Complexes with Highly Efficient Red Phosphorescence and Application to Organic Light-Emitting Diode. *J. Am. Chem. Soc.* **2003**, *125*, 12971−12979.
(68) Baek, S.-W.; Park, G.; Noh, J.; Cho, C.; Lee, C.-H.; Seo, M.-K.; Song, H.; Lee, J.-Y. Au@Ag Core−Shell Nanocubes for Efficient Plasmonic Light Scattering Effect in Low Bandgap Organic Solar Cells. *ACS Nano* **2014**, *8*, 3302−3312.
(69) Wong, K. W.; Yip, H. L.; Luo, Y.; Wong, K. Y.; Lau, W. M.; Low, K. H.; Chow, H. F.; Gao, Z. Q.; Yeung, W. L.; Chang, C. C. Blocking Reactions between Indium-Tin Oxide and Poly(3,4-ethylene dioxythiophene): Poly(styrene sulphonate) with a Self-Assembly Monolayer. *Appl. Phys. Lett.* **2002**, *80*, 2788−2790.
(70) de Jong, M. P.; van Ijzendoorn, L. J.; de Voigt, M. J. A. Stability of the Interface between Indium-Tin-Oxide and Poly(3,4-ethylenedioxythiophene)/Poly(styrenesulfonate) in Polymer Light-Emitting Diodes. *Appl. Phys. Lett.* **2000**, *77*, 2255−2257.